MICROCOPY RESOLUTION TEST CHART

NATIONAL BUREAU OF STANDARDS-1963-A
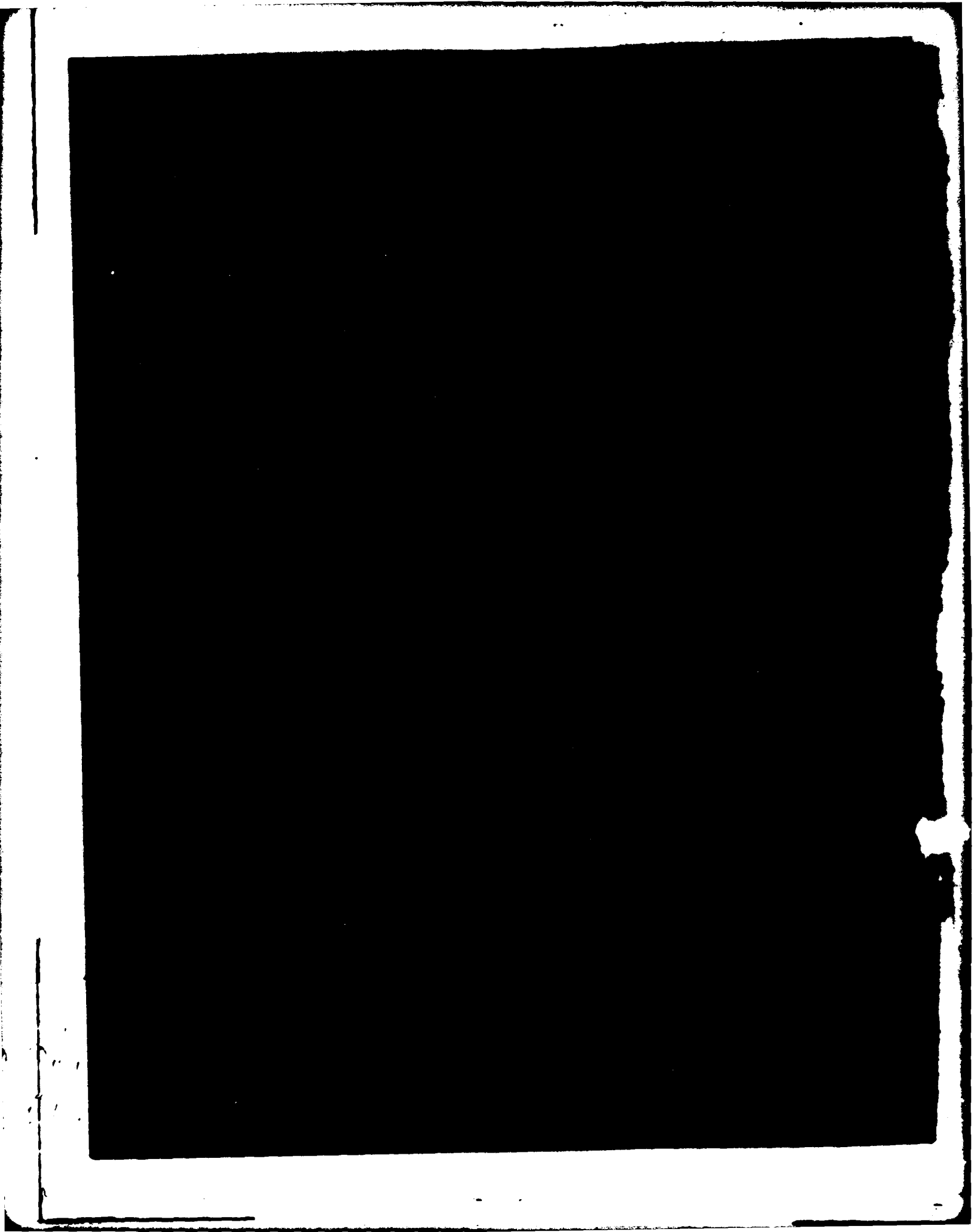
REPORT DOCUMENTATION PAGE		READ INSTRUCTIONS BEFORE COMPLETING FORM
1. REPORT NUMBER HDL-TR-1905	2. GOVT ACCESSION NO.	3. RECIPIENT'S CATALOG NUMBER
4. TITLE (and Subtitle) The Optical Processor as an Array Antenna Controller		5. TYPE OF REPORT & PERIOD COVERED Technical Report.
		6. PERFORMING ORG. REPORT NUMBER
7. AUTHOR(s) James S. Shreve		8. CONTRACT OR GRANT NUMBER(s) PRON: 1F9R0041011FA9 DA: 1L463737D181
9. PERFORMING ORGANIZATION NAME AND ADDRESS Harry Diamond Laboratories 2800 Powder Mill Road Adelphi, MD 20783		10. PROGRAM ELEMENT, PROJECT, TASK AREA & WORK UNIT NUMBERS Program Ele: 63.73.7A
11. CONTROLLING OFFICE NAME AND ADDRESS U.S. Army Materiel Development & Readiness Command Alexandria, VA 22333		12. REPORT DATE November 1979
		13. NUMBER OF PAGES 42
14. MONITORING AGENCY NAME & ADDRESS(if different from Controlling Office)		15. SECURITY CLASS. (of this report) Unclassified
		15a. DECLASSIFICATION/DOWNGRADING SCHEDULE

16. DISTRIBUTION STATEMENT (of this Report)

Approved for public release; distribution unlimited.

17. DISTRIBUTION STATEMENT (of the abstract entered in Block 20, if different from Report)

18. SUPPLEMENTARY NOTES

HDL Project: 159954
DRCMS Code: 643737.1810011

19. KEY WORDS (Continue on reverse side if necessary and identify by block number)

Coherent optical processor
Array antenna
Antenna null formation

20. ABSTRACT (Continue on reverse side if necessary and identify by block number)

Presented here are the results of an investigation into the feasibility of employing a coherent optical processor as a real-time computer for controlling a phased-array antenna. Specifically, the role of the processor was to determine the appropriate phase and amplitude distributions across the array antenna aperture. The desired antenna control included the dynamic control of antenna beam shape and position, the independent control of →

DD FORM 1473 EDITION OF 1 NOV 68 IS OBSOLETE

Item 20 (cont'd)

simultaneous multiple beams, and the independent control of antenna-pattern nulls.

FOREWORD

The investigation reported here concerns the feasibility of employing a coherent optical processor as a real-time computer for controlling the elements of a phased-array antenna. The basic concept was conceived and initially explored as part of a Harry Diamond Laboratories in-house investigation. The development of specific computational elements and their analyses was done for the Antiradiation Missile Countermeasures Group at HDL.

Accession For	
NTIS GRA&I	☑
DDC TAB	☐
Unannounced	☐
Justification___	
By___	
Distribution/	
Availability Codes	
Dist	Avail and/or special

CONTENTS

FIGURES

TABLES

7

1. INTRODUCTION

Presented here are the results of an investigation concerning the feasibility of employing a coherent optical processor as a real-time computer for controlling the elements of a phased-array antenna. The desired antenna control includes the dynamic control of antenna beam shape as well as direction, the independent control of simultaneous multiple beams, and the independent control of "holes" or antenna-pattern nulls. The steering of nulls is actually the most important aspect of the program.

The control of a planar rectangular antenna array has been treated here. No antenna elements outside the array are used to produce the nulls, nor are any specific elements dedicated to null formation. Each element is excited in such a way that the net effect of all elements is the desired pattern. Priority is given to the desired placement of nulls, which results in possible degradation of other pattern parameters such as beam shape and sidelobe levels.

Ordinary phased-array antenna control is a relatively simple task. Phased array antennas that produce a single beam of predetermined shape can be steered in azimuth and/or elevation by introducing phase shifts that progress in equal increments from column to column and/or row to row of the radiating elements. The generation of the necessary phase-shifter commands is a trivial exercise for a digital computer, and in fact, the commands required to effect several different pointing directions can easily be generated, stored, and output on a time-shared basis. The calculations required to generate the initial beam are done once, and the results are stored in the equipment, perhaps in a "hard-wired" sense.

If simultaneous multiple beams must be controlled independently, or if real-time beam-shape modifications are desired, or if independent constraints such as the location of an antenna pattern null are introduced, the real-time computation load increases drastically. It appears that several iterations of two-dimensional Fourier transforms are required for each new pointing direction or pattern modification. One candidate algorithm incorporates three two-dimensional Fourier transforms plus two sets of element-by-element complex multiplications. A two-dimensional fast Fourier transform requires about $N^2(\log_2 N^2)$ complex multiplications, where N is the number of elements along each side of the array. For the entire algorithm, there is a total of $N^2[3(\log_2 N^2)+2]$ complex multiplications. This means, for example, that an array of 100 elements by 100 elements would require $\frac{1}{4}$ million complex multiplications for each update.

The heavy computation load imposed upon an all-digital antenna controller led to the consideration of the coherent optical processor as a computational element in this role. With the coherent optical processor, two-dimensional Fourier transforms and element-by-element multiplications are essentially done instantaneously. However, data handling and optic-to-electronic interfacing require time and must be implemented by digital circuitry. With the HDL breadboard controller, the computation load for implementing the above algorithm is equivalent to between one and two times N^2 complex multiplications. Thus, for a 100 by 100 element array, the digital computation load is about 4 percent of the all-digital system. For a 32 by 32 array, it is about 5 percent. (The digital computational load would be far less if the more advanced electro-optic interface described in section 6 were incorporated.)

2. SUMMARY

A coherent-optical-processor algorithm for the control of the elements of an array antenna has been developed and demonstrated with laboratory hardware. Two-dimensional binary func-

tions for antenna test patterns, other constraining functions required by the processor, and the basic nulling functions were derived and put in the form of high-resolution photographic plates. These plates were then used to gather experimental data with the existing coherent-optical-processor hardware. The output from the processor—the phase and amplitude levels to be imposed on each antenna element—was in the form of digital punched tape. By reducing these data with an existing digital computer program for antenna-pattern synthesis, the patterns that would have been produced by an antenna under the control of the coherent optical processor were obtained in graphical form.

Using this experimental approach, independent beam and null control was demonstrated, and achievable null depth was measured. With the first and simplest nulling functions, null depth was disappointingly slight (see fig. 9 and 10, p. 19). With a more advanced nulling function based upon sampling theory, a null depth of -43 dB was achieved (see fig. 20, p. 27). It appears that greater null depth should be attainable with larger arrays and/or greater resolution in the control of excitation amplitude and phase.

Analyses were made which relate null depth to amplitude quantization, phase quantization, and photodetector noise. It was found that amplitude and phase control are about equally important in the generation of nulls, which means that "phase control only" results in nulls that are halfway between no null and a perfect null—that is, only 3 dB down.

Quantization effects appear as a residual pattern amplitude at the null position. For an amplitude quantization of "b" bits in an antenna array of "m" elements, this residual level is about $(-4.8 \text{ dB} - 6.0b \text{ dB} - 10 \log_{10} m \text{ dB})$ below the main beam peak. For a phase quantization of "b" bits, the residual level is about $(11.2 \text{ dB} - 6.0b \text{ dB} - 10 \log_{10} m \text{ dB})$ below peak. It is assumed that the null is reasonably far displaced from boresight, and that the array amplitude distribution is more or less uniform.

3. BASIC ARRAY CONTROLLER

3.1. Theory

The far-field directivity pattern exhibited by a planar antenna aperture and the E-field distribution within the aperture are related by the two-dimensional Fourier transform. The directivity pattern must be expressed as a function of direction cosines, and a cosine correction factor must be introduced for the nonisotropic radiation of each element E-field, in order for a Fourier transform relationship to hold precisely over the entire range of pattern angles.

We will adopt the usual notation of lower-case letters denoting variables and functions of interest (here relating to antenna patterns), upper-case letters denoting corresponding variables and functions of the Fourier transforms (here relating to aperture excitation), and $\mathcal{F}$ denoting an operator which takes the Fourier transform. As in figure 1, the aperture is assumed to lie in the X-Y plane with an excitation field vertically polarized, while α and β define a direction of radiation from that aperture.

The complex directivity pattern is given by

$$f'(x, y) = \cos \alpha \, \mathcal{F}^{-1}\{F(X, Y)\} = \cos \alpha \, f(x, y) \quad , \tag{1}$$
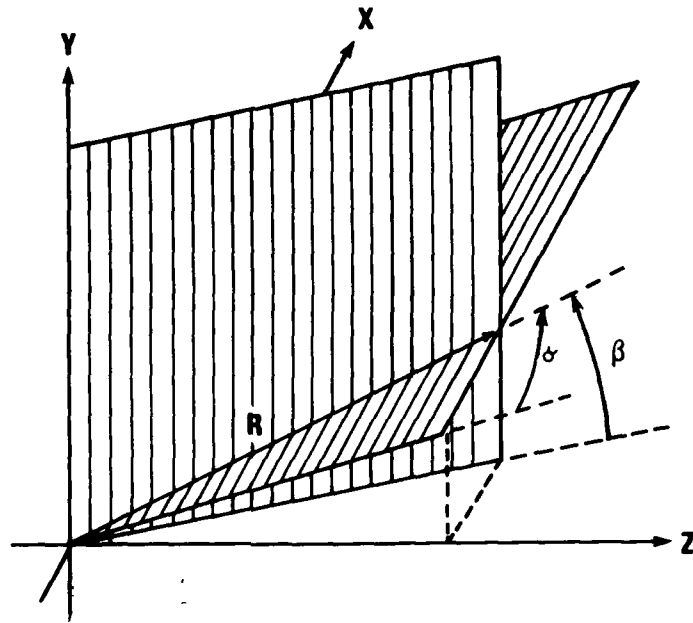
Figure 1. Coordinate system.

where

    $f'(x, y)$ is the pattern amplitude per unit solid angle, x and y being variables proportional to direction cosines and actually defined as $(\sin \alpha)/\lambda$ and $(\sin \beta)/\lambda$, respectively, and

    $F(X, Y)$ is the field amplitude distribution within the aperture.

In the case of array antennas, each discrete element of the array may be considered a point source, and the "correction factor" is then merely the radiation pattern of the element. This is the case explored here. Further, it is assumed that there is a single (and known) function g' which closely approximates the directivity pattern of each element for a given array, as that element radiates in the presence of the other elements. The array pattern thus becomes

$$f'(x, y) = \mathscr{F}^{-1}\{G(X, Y)\star H(X, Y)\} = g'(x, y)\cdot h(x, y) \quad , \tag{2}$$

where

    G is the equivalent aperture excitation for a single element and

    H is a replicating and weighting function or "array excitation."

Specifically, we have

$$\mathscr{F}^{-1}\{G(X, Y)\} = g'(x, y) \tag{3}$$

11

and

$$H(X, Y) \equiv \sum_{m,n} \delta[(X - X_m), (Y - Y_n)] \cdot F_w(X_m, Y_n) \quad , \tag{4}$$

where $F_w(X_m, Y_n)$ specifies the relative phase and amplitude exhibited by the element at X_m, Y_n.

The antenna array controller essentially does the inverse of the antenna—that is, given a far-field pattern, it deduces the array excitation H which would be required to produce it. The weighting factor F_w is the output of the controller. The output thus assumes the role of "instructions" to be sent to the antenna undder control. The instructions specify the relative phase and amplitude that each element of the array must assume. The instructions are updated in real time so that the antenna can be dynamically controlled.

Although any arbitrary far-field pattern can be specified as an input to the controller, the actual array antenna is limited in performance because of its finite extent and nonzero element spacing. For the usual case of half-wavelength element spacing, the limitation becomes one of extent only. For a rectangular aperture, the effect in the far-field is to produce a pattern that is the convolution of the arbitrary input pattern and a two-dimensional sinc function. (By definition, $\text{sinc}(x, y)$ equals $(\sin \pi x)/(\pi x) \cdot (\sin \pi y)/(\pi y)$.) An array of size A and B exhibits an array excitation $H_{A,B}$, which produces the pattern $f'_{A,B}$, given by

$$f'_{A,B}(x, y) = \mathscr{F}^{-1}\{G(X, Y) \star H_{A,B}(X, Y)\} \quad , \tag{5}$$

where

$$H_{A,B}(X, Y) = \text{rect}\left(\frac{X}{A}, \frac{Y}{B}\right) \cdot H(X, Y) \quad , \tag{6}$$

and thus

$$f'_{A,B}(x, y) = A \cdot B \cdot f'(x, y) \star \text{sinc}(xA, yB) \tag{7}$$

From equations (2) and (6),

$$H_{A,B}(X, Y) = \text{rect}\left(\frac{X}{A}, \frac{Y}{B}\right) \cdot \mathscr{F}\{f'(x, y)/g'(x, y)\} \tag{8}$$

in the regions where $g' \neq 0$. Equation (8) describes the operations that the antenna controller performs in its basic operating mode.

3.2. Implementation

The coherent optical processor is based upon that property of lenses by which the Fourier transform of any coherent optical image applied at the front focal plane is imaged at the rear focal plane. In the test-bed antenna controller, as shown in figure 2, the input directivity pattern f' is applied by illuminating with laser light a high-resolution photographic plate whose transmittance variations represent the desired function. Beam steering is accomplished by translating the plate. Division by the element pattern g' is accomplished by a second (stationary) plate whose opacity represents the appropriate function. In the transform plane a rectangular aperture, essentially a scaled model of the antenna array, performs the rect multiplication which truncates the array.
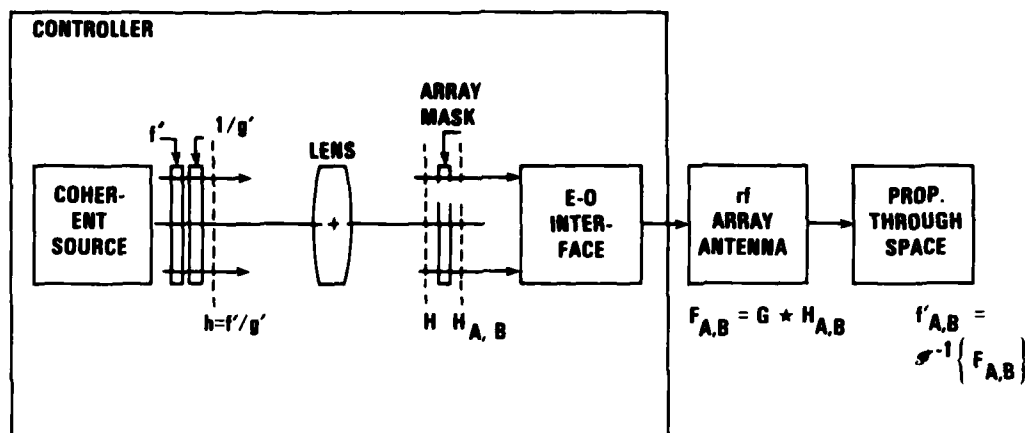
12

Figure 2. Flow chart for basic controller.

The output phase and amplitude values F_w are recovered in the form of electronic signals by an implementation of the HDL "electro-optic phase-measuring device," referred to here simply as the "E-O interface." This device comprises a photodiode-array camera and a microprocessor, and incorporates a coherent planar reference beam which is phase modulated and mixed with the optical output at the photodiode array. The timing of the difference-frequency zero crossings, as seen at each photodiode, provides the desired relative phase information. Of course, amplitude is readily measured.

The existing E-O interface requires six rasters of data (six sample points in time for each of the 1024 photodiodes) to permit filtering and phase determination. As described in section 6, a new interface has been designed wherein only one raster of data need be taken for each data update.

Figure 3 (p. 14) shows details of a configuration in which several antenna "beams" can be controlled simultaneously, or several overall patterns can be controlled sequentially.

3.3. Experimental Results for Basic Control

Experimental data ("instructions") were taken using the equipment described in appendix A. The instructions were evaluated in nonreal time by digital computer, using a pattern synthesis and plotting program. The instructions were transferred from the antenna controller to the evaluation computer by means of paper tape punched under control of the antenna-controller support electronics.

The hypothetical antenna to be controlled was a 32 by 32 array of omnidirectional elements spaced at $\frac{1}{2}$ wavelength. It was assumed that both phase and amplitude of each element was controllable, and therefore 2048 phase and amplitude values were output for each pattern.

The first tests served only to confirm that antenna beam shape and pointing direction were controllable. Figure 4 (test No. 5) shows the computer-plotted pattern obtained when the input

13
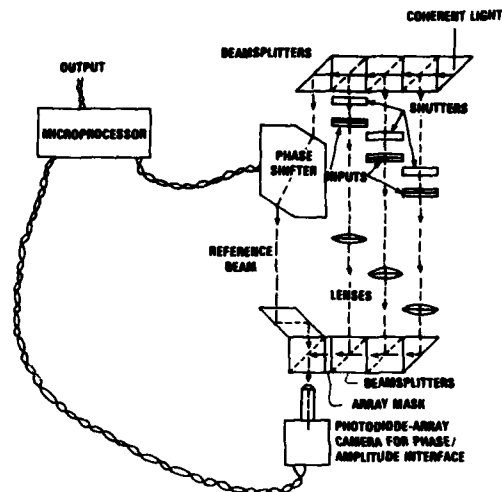
Figure 3.   Multi-beam antenna controller.

pattern was a cylindrical function with a scaled full-angle of 3.57 deg. (Recall that the hypothetical array is 16 wavelengths on a side.) Figure 5 (test No. 6) represents the same beam, but steered off boresight by 11 deg. Figure 6 (test No. 10) shows the results of an annular input mask designed to reduce sidelobes. Here the beam had been steered so as to locate the first sidelobe on boresight, which was the first part of an exercise wherein a null was subsequently imposed on boresight.
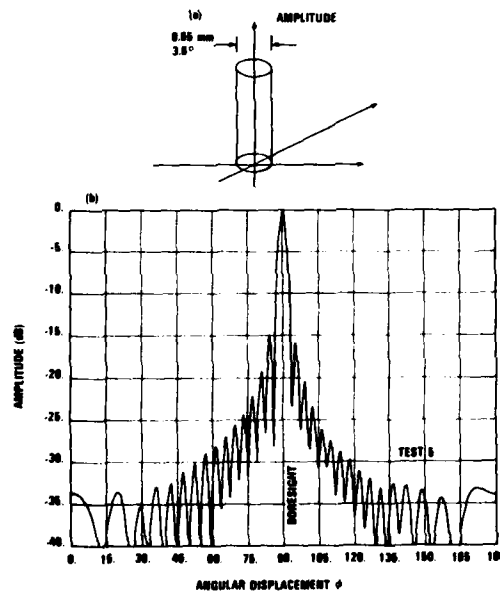
Figure 4.   Test using input pattern A: (a) input pattern and (b) synthesized output pattern.

14
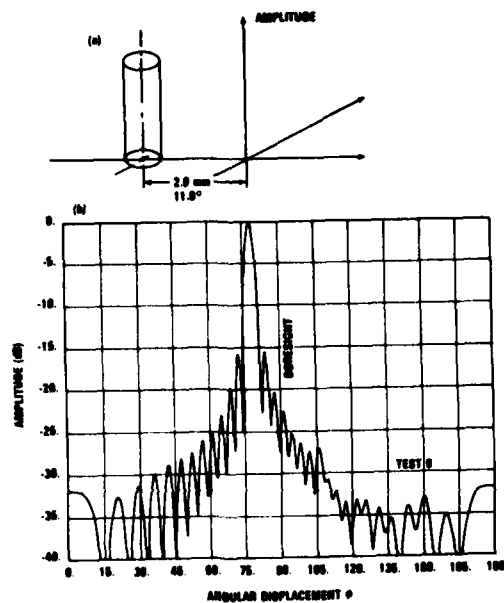
Figure 5.   Test using input pattern A, translated: (a) input pattern and (b) synthesized output pattern.
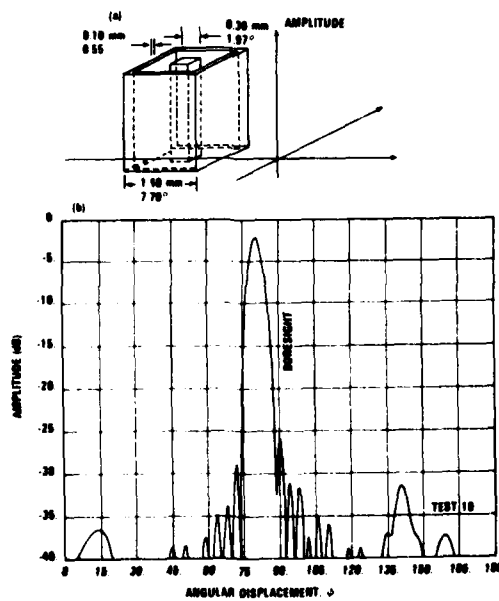
Figure 6.   Test using input pattern C, translated: (a) input pattern and (b) output pattern.

15

In order to confirm proper operation of the optics and the E-O interface, an approximation to equation (7) was programmed and run on a digital computer. The theoretical output pattern obtained in this manner for input pattern A was compared with the pattern obtained when the antenna controller "instructions" were analyzed. The theoretical estimate placed the -3 dB point at a half-angle of 1.67 deg, the first zero crossing at a half-angle of 3.85 deg, and the first sidelobe level at 15.3 dB below peak. These values agree with the antenna controller results as closely as these values can be read on the plot.

In the beam steering exercise, the controller pattern was translated a scale 2.0 mm, which corresponds to 11.0 deg. (In the HDL experimental setup, angle off boresight is the arcsine of controller displacement divided by 10.45 mm.) Again this agrees with the experimental results as shown in figure 5, if we take into account the initial boresight error shown in figure 4. (No attempt had been made to precisely locate boresight, since relative displacement was the primary concern.)

4. NULL FORMATION

4.1. General

It was desired to include in the antenna controller the capability to modify its instructions in such a way that the antenna would exhibit deep pattern nulls in desired arbitrary directions independent of other pattern considerations. In the case of a pencil beam pattern, for example, null position must not be affected when the beam is moved, and the beam position must not be affected when the null is moved.

In order for the nulls to exhibit the desired depth, it became obvious that the null constraint must be imposed in the processor after the other pattern constraints are imposed—i.e., it must be a "null-priority" processor. Otherwise, the attempt to form the desired pattern obliterates the nulls. The controller was therefore configured as shown in figure 7b, with $h_2 = h_{A,B}$, and in figure 8.

In figure 7a we see that the addition of lenses 2 and 3, which effect an inverse Fourier transform followed by a Fourier transform, leaves the basic controller operation unchanged. Imposing array mask 2 likewise has no effect on H_2, as is apparent from equation (6). In figure 7b, however, a constraining filter is imposed in the plane where h_2 is formed, thereby altering the far-field pattern within the controller in an attempt to produce a null in the final resulting antenna pattern. Note that as for the basic controller, the resulting pattern, here f_4', experiences a convolution with a sinc function:

$$f_4' = \mathscr{F}^{-1}\{G \star H_4\} \quad . \tag{9}$$

and

$$\mathscr{F}^{-1}\{H_4\} = A \cdot B \cdot (h_2 \cdot f_c) \star \operatorname{sinc}(xA, yB) \quad . \tag{10}$$

This convolution, of course, is what precludes a point "null" or zero in f_c from establishing a deep null in the resulting pattern.

There are at least three approaches to the design of a constraining filter that will tend to produce a null. In the simplest approach, a localized area (of the image) of h_2 is merely blocked by a filter having an opaque spot of a shape and size calculated to best effect a null in the final pattern. This approach was implemented experimentally and is reported on in section 4.2.
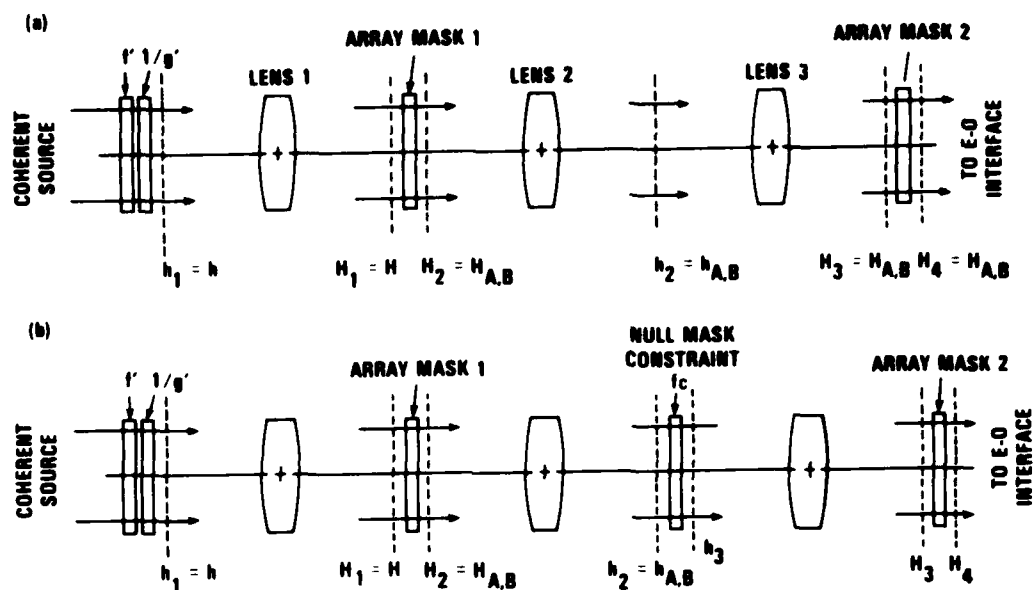
16

Figure 7. Flow chart for iterative configuration: equivalent to (a) basic controller and (b) controller with null-producing mask.
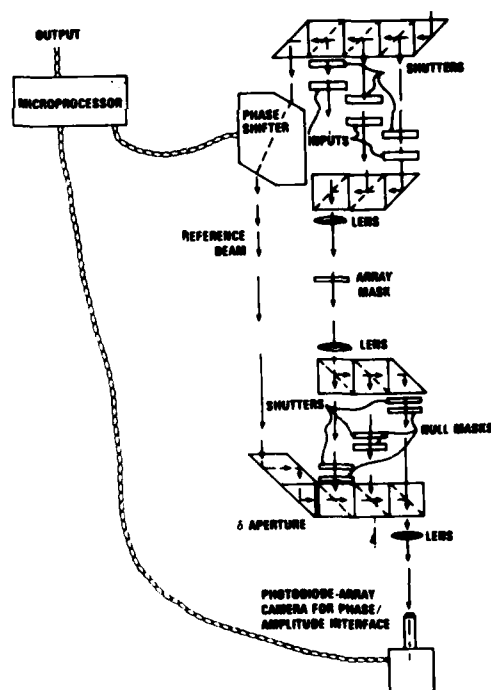

Figure 8. Multi-beam antenna controller with null control.

In a more refined approach, the localized area of h_3 is algebraically inverted and weighted by a filter which selectively phase shifts and attenuates the image of h_2. Here the localized area can be made smaller, which should improve performance. The drawbacks are the reduction in available optical energy caused by the filter attenuation, and the difficulty of fabricating a phase-controlling filter. No experimentation was done with this approach because of the fabrication difficulty, but the theory of operation is given in section 4.3.

The third approach is perhaps more elegant, and has produced the best experimental results. In this case h_2 is "sampled" by a filter which consists of a two-dimensional array of clear apertures in an opaque background. With proper scaling, the deletion of a sample (blocking of an aperture) will produce the desired null (see sect. 4.4).

4.2. Pattern Blocking

Consider a constraining function f_c of the form $1 - f_d$, where f_d is a very narrow function of unity area. Thus,

$$h_4 = [h_2 \cdot (1 - f_d)] \star \text{sinc}(xA, yA) \quad . \tag{11}$$

From the definition of h_2 (see eq. (6)), and the realization that the self-convolution of a sinc function is the same sinc function, we find

$$h_4 = h_2 - [(h_2 \cdot f_d) \star \text{sinc}(xA, yA)] \quad . \tag{12}$$

If f_d could be realized as a Dirac function, $\delta(x - x_0, y - y_0)$, we would have

$$h_4 = h_2 - h_2(x_0, y_0) \star \text{sinc}(xA, yA) \quad . \tag{13}$$

Clearly, at x_0, y_0 the function h_4 would be zero. The price paid for this null is the degradation in the nearby pattern caused by the subtraction of the "sidelobes" of the sinc function.

In reality, the Dirac function can only be approximated, as by a narrow rect function, for instance. Thus we set

$$f_d = \text{rect}[(x - x_0)/r, (y - y_0)/s] \quad . \tag{14}$$

which has the effect of degrading the null somewhat.

If the rect dimensions r and s are so small that h_2 is nearly constant inside the rect "pulse," we have

$$h_4/h_2 \approx 1 - (\text{rect}[(x - x_0)/r, (y - y_0)/s] \star \text{sinc}(xA, B)) \quad . \tag{15}$$

and

$$(h_4/h_2)|_{x_0, y_0} \approx 1 - \int_{-s/2}^{s/2} \int_{-r/2}^{r/2} \text{sinc}(xA, yB) \, dx \, dy \quad . \tag{16}$$

To determine r and s we set this last expression equal to zero:

$$0 = 1 - \int_{-s/2}^{s/2} \int_{-r/2}^{r/2} \text{sinc}(xA, yB) \, dx \, dy \quad . \tag{17}$$

Equation (17), which specifies r and s for the configuration referred to as "Null Mask A," no longer involves $h_{A,B}$ or x_0 and y_0. This means that the size (and shape) of the zero region is

18

fixed, while its location is specified by the desired null location in the actual antenna pattern. In practical terms, a photographic slide with transmittance representing f_c can be fabricated and inserted in the controller. The slide can be translated to steer the resulting null. In practice the performance of this mask is severely limited, as $h_{A,B}$ is not generally constant, even over the small region blocked, as assumed.

An experimental Null Mask A slide was fabricated photographically and tested using the same techniques as in the basic controller tests (see sect. 3.3). Figures 9 and 10 show typical results when this mask is employed. Here a null was imposed on the first sidelobe of the antenna patterns shown in figures 5 and 6.

The null depth was disappointingly slight. This performance was analyzed by digital computer, using comparable sinc patterns instead of the actual patterns, for convenience. The null depth achievable is highly dependent on the beam shape near the null and on the exact dimensions of the mask. The former is illustrated in figure 11, and the latter is shown in table I.
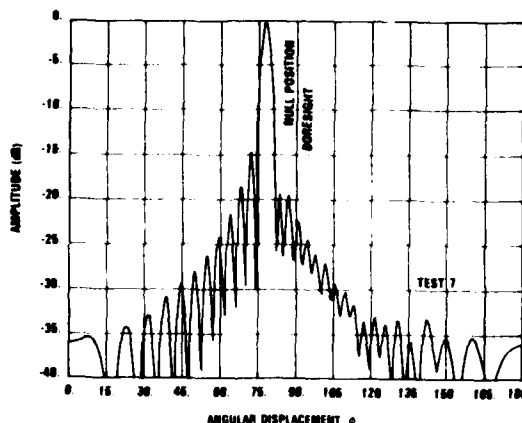
Figure 9. Synthesized output for pattern A and null mask A.
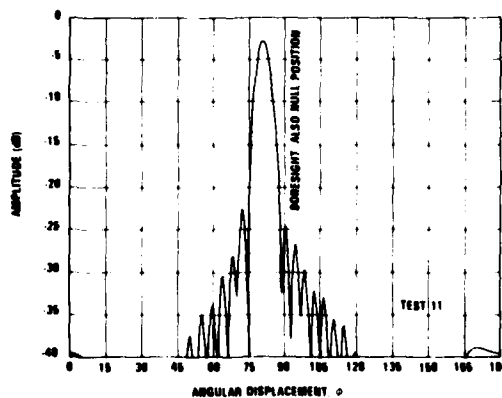
Figure 10. Synthesized output for pattern C and null mask A.

19
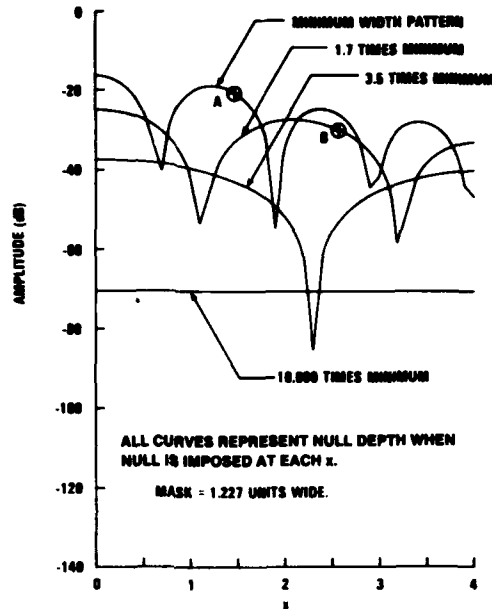
Figure 11.   Sinc pattern, null mask A (where *x* is proportional to direction cosine).

TABLE I
Null Depth for Various Mask Widths, with Null on Boresight

Antenna pattern width	Mask width (% of nominal[a])	Amplitude at null (dB)
1	90	−14.5
	95	−15.4
	100	−16.2
	105	−17.0
	110	−17.7
1.7	90	−19.2
	95	−21.7
	100	−24.9
	105	−29.3
	110	−36.9
3.5	90	−22.5
	95	−27.3
	100	−37.4
	105	−37.4
	110	−28.4

[a] Nominal width = 1.227 in the normalized coordinate system. Normalized coordinates, divided by 16, give the sine of angular coordinates.

20

Figure 11 displays the theoretical pattern amplitude, relative to peak amplitude, at the null location as a function of null location. Null location is given in terms of the generalized coordinate X. For the 16- by 16-wavelength array considered, the angle off boresight is given by arcsine ($X/16$). The curve labeled "uniform excitation pattern" pertains to the beam that would be formed by a uniformly illuminated, constant-phase array excitation. The other curves are merely wider scaled versions of this. The points marked "A" and "B" correspond to the experimental null positions employed in figures 9 and 10, respectively.

Table I shows null depth as a function of the width of the masking area (or region of zero value) in Null Mask A, for each of the input patterns used in figure 11. The null location is on boresight in each case. The nominal width of the masking area is the value obtained from equation (12).

4.3. Pattern Subtraction

Consider the constraining function

$$f_c = k - (1 + k) \, \text{rect}[(x - x_0)/r, (y - y_0)/s] \quad , \tag{18}$$

where k is a constant less than unity. (Such a function might be implemented by coating a glass plate with an attenuating layer with transmittance k^2 and a phase-shifting layer with a relative phase shift of π radians, both covering the entire plate except where the null is specified.) The equation corresponding to equation (16) is then

$$(h_4/h_2)|_{x_0 y_0} \approx k \left\{ 1 - [(1 + k)/k] \int_{-s/2}^{s/2} \int_{-r/2}^{r/2} \text{sinc}(xA, yB) \, dx \, dy \right\} \quad . \tag{19}$$

By properly adjusting k, a null can be formed, as is evident from the above, with smaller r and s.

4.4. Pattern Sampling

The most promising (and in retrospect the most obvious) technique for producing nulls is based upon sampling theory. Although usually associated with one-dimensional time-varying functions, sampling theory can of course be applied to two-dimensional functions of spatial coordinates, such as antenna patterns. Thus, provided the antenna pattern is band-limited (we refer here to spatial frequencies in two dimensions), all the information in the pattern is preserved in a properly spaced matrix of (complex-amplitude) point samples. Furthermore, the original pattern can be reconstructed by convolving the array of point samples with a properly scaled two-dimensional sinc function.

Any antenna pattern generated by a finite aperture is band-limited in the proper sense, if the antenna pattern is expressed in terms of direction cosines (or sines of the angular complements), which is the case within the antenna controller. Secondly, and not by coincidence, the finite size of the antenna aperture effects a convolution with a sinc function which is precisely the proper interpolation function for reconstructing a pattern sampled at the Nyquist rate. (This convolution is actually the cause of the null degradation seen in the previous nulling technique.)

Assuming a pattern is sampled at the Nyquist rate, the value of the reconstructed pattern at any sample point depends solely upon the one sample taken at that point, and not on any of the

21

other samples. This is because the sinc interpolation function for any one sample has zero crossings at every other sample location, and hence contributes nothing at those exact locations.

The above suggests a technique for forcing a null in the antenna pattern at a given location, yet leaving the remainder of the pattern largely undisturbed—at least undisturbed at a number of specific points. The approach is to form, within the antenna controller, the far-field pattern without null, then to "sample" this pattern by interposing a mask in the form of a regularly spaced matrix of very small apertures. The sample where the null is to be formed is suppressed, which means that the aperture at that location is merely blocked off. The following operations (taking the Fourier transform, imposing the array size limitation, transferring the phase and amplitude information to the real antenna elements, and forming the real antenna pattern) all amount to a sinc interpolation of the set of samples. At each sample point, except one, the pattern without null is faithfully reproduced. At the point where the sample is suppressed, the pattern is forced to zero. Of course the null can be moved to a new location by translating the sample mask.

In figure 7b, the function h_2 is the far-field pattern without null, except for the factor g' which represents the pattern of the array element itself. Now $h_{A,B}$ is the function that will be sampled, and therefore must be band limited. Recalling that the transform of h_2, which is in the "frequency domain," was the result of truncating a function H (see eq. (6)), we see that h_2 is indeed limited to the spatial frequencies $-\frac{1}{2}A$ to $\frac{1}{2}A$ and $-\frac{1}{2}B$ to $\frac{1}{2}B$. At the Nyquist rate the sample spacing is $1/A$ in one coordinate and $1/B$ in the other. The sampling function will therefore be

$$f_c = \sum_i \sum_j \delta(x - x_0 - i/A)\delta(y - y_0 - j/B) \quad . \tag{20}$$
$$\scriptstyle i\neq 0 \; j\neq 0$$

The required interpolation function is of course sinc(xA, yB), which is just the transform of the array mask. The resulting pattern is gotten from equations (9) and (10), and is found to be

$$f'_4(x, y) = g'(x, y)\{h_2(x, y) - h_2(x_0, y_0) \, \mathrm{sinc}[(x - x_0)A, (y - y_0)B]\} \quad . \tag{21}$$

This is the desired pattern with a "sinc-shaped" null centered at x_0, y_0.

In the actual antenna controller, the function f_c, as given by equation (20), cannot be implemented. Instead, an approximation must be made to the Dirac functions, such as narrow rect functions. Therefore let

$$f_c = \sum_i \sum_j \mathrm{rect}[(x - x_0 - i/A)/r] \cdot \mathrm{rect}[(y - y_0 - j/B)/s] \quad . \tag{22}$$
$$\scriptstyle i\neq 0 \; j\neq 0$$

The smaller the aperture dimensions r and s are, the more closely this function approximates that of equation (20), but the more optically attenuating the physical mask becomes. The optical power available and the photodetector sensitivity in the antenna controller impose a limit on the attenuation that can be tolerated.

An analysis was made which consisted of evaluating equation (21) at various null positions by digital computer approximations. Various width antenna patterns are assumed.

Figures 12, 13, and 14 show the residual null amplitude, as well as the pattern amplitude without null, for sampling aperture widths of 10, 30, and 50 percent of sample spacing, respec-
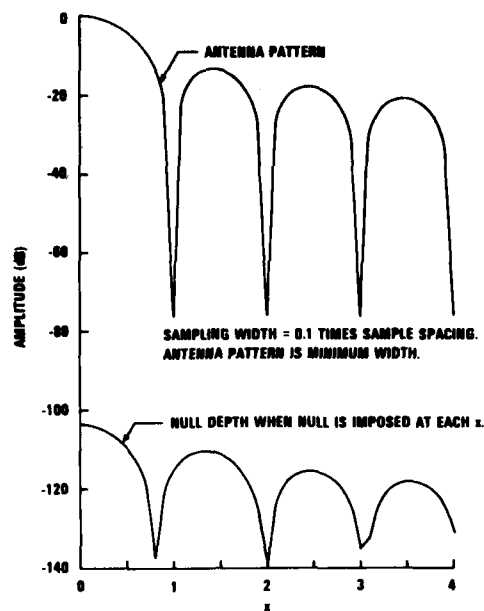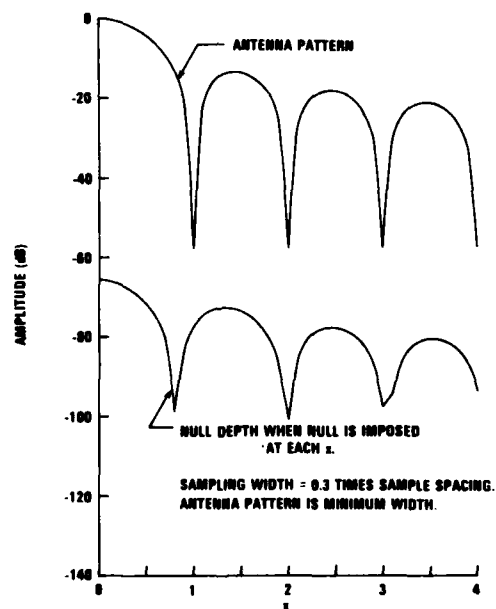
22

Figure 12.   Minimum-width sinc pattern, point array sampling with sampling width of 10 percent (where *x* is proportional to direction cosine).

Figure 13.   Minimum-width sinc pattern, point array sampling with sampling width of 30 percent (where *x* is proportional to direction cosine).
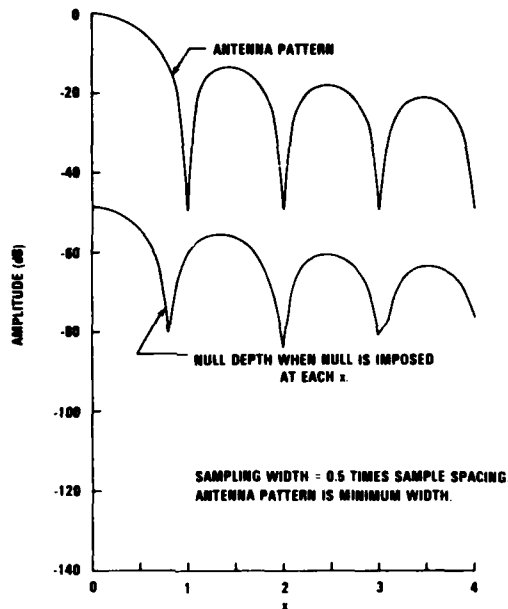
23

Figure 14. Minimum-width sinc pattern, point array sampling with sampling width of 50 percent.

tively, where the basic antenna pattern is minimum width. Bear in mind that the null amplitude shown at a given x is the amplitude that would be observed if the nulling function were centered at that x. Here again the coordinate x can be converted into the angle off boresight by taking the arcsine of $(x/16)$.

Figure 15 shows the effects of changes in antenna beam width for a sampling aperture width of 30 percent of sample spacing.

In order to determine the precision required in manufacturing the sampling mask and in maintaining proper optical focal lengths and lens distances, the effects of improper sample spacing (or apparent spacing) were investigated. Figures 16, 17, and 18 show that a 1-percent tolerance still produces good results.

Multiple nulls can be accommodated under either of two conditions: (a) they are spaced at distances that are exact multiples of the sample spacing, in which case more than one sample is deleted, or (b) they are spaced far apart so that the formation of one null does not fill in another null. A means for implementing widely spaced nulls is shown in figure 19. Here the image of the pattern is first sampled with one sample deleted, then reconstructed, and finally sampled again with one deleted.

An experimental sampling mask with suppressed samples was fabricated photographically and tested as before (see sect. 3.3). Figure 20 shows the results when an attempt was made to place a null near the peak of the first sidelobe. The controlled antenna was assumed to have 900 elements, 30 on a side. The amplitude data were quantized to 6 bits; the phase data were quantized

24
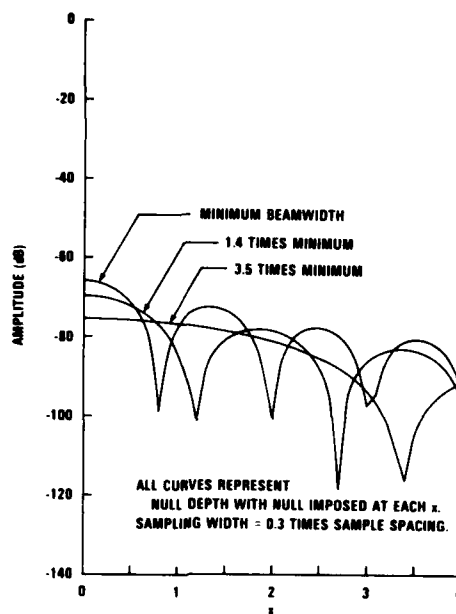
Figure 15. Sinc pattern, point array sampling, with various beam widths, and with sampling width fixed at 30 percent.

Figure 16. Minimum width sinc pattern, point array sampling, 1-percent sample spacing error effect for sample width of 10 percent.

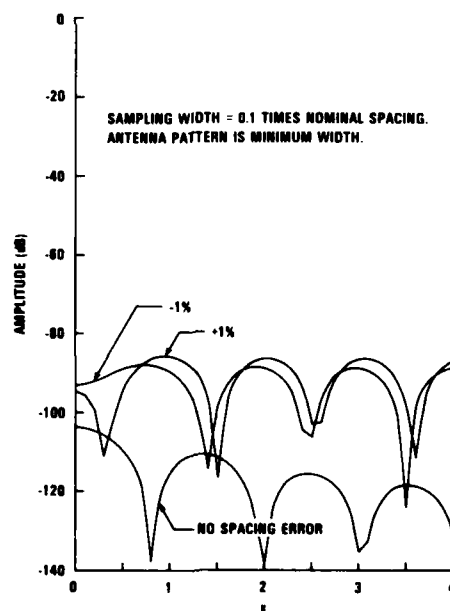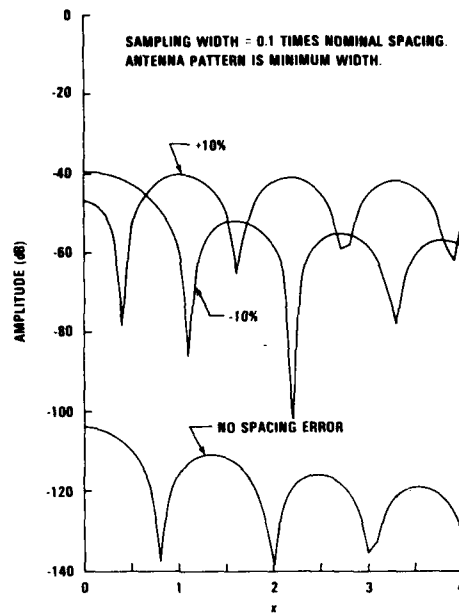Figure 17. Minimum-width sinc pattern, point array sampling, 10-percent sample spacing error effect for sample width of 10 percent.
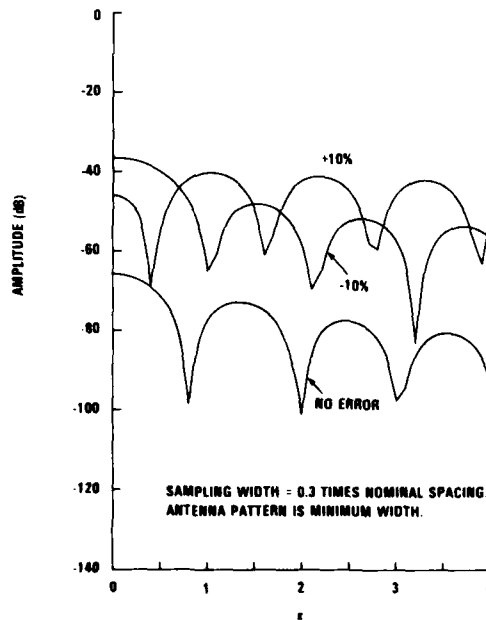
Figure 18. Minimum-width sinc pattern, point array sampling, 10-percent sample spacing error effect for sample width of 30 percent.

26
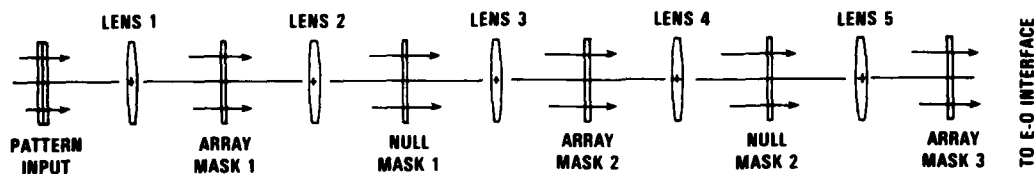
Figure 19. Configuration for effecting independently positioned (but well separated) simultaneous nulls.
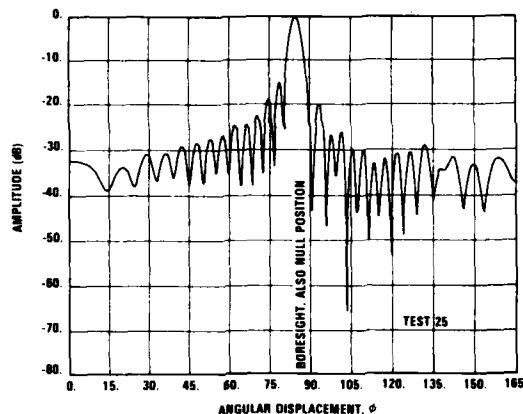
Figure 20. Synthesized output for pattern A and sampling-type null mask.

to 8 bits. The photodetector noise was 4 bits below average signal. The sampling filter had clear apertures that were 30 percent of the aperture spacing.

The predicted null depth, based on an analysis of noise, quantization (see sect. 5), and nonzero sample size is about 52 dB below the pattern peak; the measured depth is about 43 dB. The discrepancy appears to be due to stray diffracting particles which were within the experimental optical system.

5. NULL ERROR ANALYSIS

5.1. Phase-Only Control

The following analysis is based upon an antenna controller incorporating a sampling-array type of null mask. The nulling is accomplished by deleting one sample of the far-field pattern $a(x, y)$. This causes the pattern to behave as if an oppositely phased antenna were introduced at the position of the deletion, with just the proper amplitude to cancel the original pattern (see fig. 21).

For the simple case of uniform aperture illumination for each pattern, the two patterns may be expressed as

$$a_1 = k_1 \operatorname{sinc}[(x - x_0)/r, (y - y_0)/s] \tag{23}$$

27

ORIGINAL PATTERN

PATTERN INTRODUCED BY SAMPLE DELETION
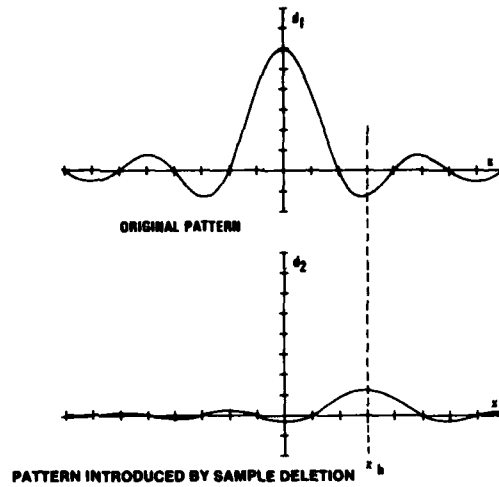
Figure 21. Component antenna patterns for producing a null.

and

$$a_2 = k_2 \operatorname{sinc}[(x - x_n)/r, (y - y_n)/s] \quad , \tag{24}$$

where

$$k_2 = -a_1(x_n, y_n) \quad . \tag{25}$$

The total pattern is $a = a_1 + a_2$, which obviously displays a null at x_n, y_n. The Fourier transform of "a" is the total aperture excitation "A," given by

$$A = rs \operatorname{rect}(Xr, Ys)R \quad , \tag{26}$$

where

$$R \equiv k_1 \exp[-2\pi i(Xx_0 + Yy_0)] + k_2 \exp[-2\pi i(Xx_n + Yy_n)] \quad . \tag{27}$$

In polar form,

$$R = |R| \exp[-2\pi i(Xx_0 + Yy_0)] \exp(i\phi) \tag{28}$$

where

$$|R| = [k_1^2 + k_2^2 + 2k_1 k_2 \cos(2\pi[X(x_n - x_0) + Y(y_n - y_0)])]^{1/2} \tag{29}$$

and

$$\phi = \tan^{-1}\left[\frac{k_2 \sin(2\pi[X(x_n - x_0) + Y(y_n - y_0)])}{k_1 + k_2 \cos(2\pi[X(x_n - x_0) + Y(y_n - y_0)])}\right] \quad . \tag{30}$$

Clearly R, and therefore the desired aperture excitation, exhibits amplitude modulation as well as phase modulation. If the antenna elements are not spatially modulated in amplitude, then the resulting pattern will be some new function $b(x, y)$. The pattern $b(x, y)$ can be determined

28

from the altefed form of aperture excitation:

$$b(x, y) = \mathscr{F}\left\{ rs \, \text{rect}(Xr, \, Ys)\frac{R}{|R|}\right\} \quad . \tag{31}$$

A measure of effectiveness of the fixed-amplitude array excitation is the ratio of the pattern amplitude in the null direction to the pattern amplitude on boresight: i.e., $|b(x_n, \, y_n)/b(x_0, \, y_0)|$.

Fortunately, for cases of interest, $|k_2|$ will be small compared to $|k_1|$. The highest value that $|k_2|$ will assume (unless the null is positioned within the antenna main beam) is $0.22|k_1|$, which is the peak amplitude of the first sidelobe. In general, $|k_2|$ will be much smaller than this, which permits the following approximation:

$$\phi \approx (k_2/k_1) \sin\{2\pi[X(x_n - x_0) + Y(y_n - y_0)]\} \quad . \tag{32}$$

The transform of the aperture excitation now becomes slightly more manageable:

$$b(x, y) \approx J_0(k_2/k_1) \, \text{sinc}[(x - x_0)/r, \, (y - y_0)/s]$$
$$+ \, J_1(k_2/k_1) \, \text{sinc}[(x - x_n)/r, \, (y - y_n)/s]$$
$$- \, J_1(k_2/k_1) \, \text{sinc}[(x - 2x_0 + x_n)/r, \, (y - 2y_0 + y_n)/s] + \ldots \tag{33}$$

The ratio of amplitude at the null position to the peak amplitude is then given by

$$\frac{b(x_n, \, y_n)}{b(x_0, \, y_0)} \approx \frac{J_0(k_2/k_1) \, \text{sinc}[(x_n - x_0)/r, \, (y_n - y_0)/s] + J_1(k_2/k_1)}{J_0(k_2/k_1) + J_1(k_2/k_1) \, \text{sinc}[(x_n - x_0)/r, \, (y_n - y_0)/s]} \quad . \tag{34}$$

But

$$(k_2/k_1) = -\text{sinc}[(x_n - x_0)/r, \, (y_n - y_0)/s] \quad , \tag{35}$$

which leads to

$$\left|\frac{b(x_n, \, y_n)}{b(x_0, \, y_0)}\right| \approx \frac{1}{2}\left|\frac{k_2}{k_1}\right| \quad . \tag{36}$$

This says that for small $|k_2/k_1|$, only half the antenna-pattern amplitude is nulled out at the intended null position if only the phase of the array elements is controlled.

5.2. Amplitude Quantization

We will assume that the range of excitation amplitudes to be fed to the various elements of the array is large compared to the resolution of the amplitude quantizer. The effect of the quantization is then one of introducing an "error signal" at each element, with each error signal having an amplitude probability density constant over the range of one quantum. We will statistically combine the effects of each error signal to find the net effect of the quantization.

Only in the direction of the intended pattern maximum (a degenerate point in terms of quantization effects) do the contributions from all the array elements sum together in phase. At the point of interest (the intended null position), the contributions with their various phase angles essentially sum to zero. If the intended null position is displaced from the intended pattern maximum beyond the first pattern zero crossing, then the various contributions from the array of elements will exhibit a range in phase in excess of 2π. For cases of interest, it may be

29

reasonably assumed that the phases of the element contributions, and specifically the phases of the error signals, are more or less uniformly distributed over all angles. The expected value of the rms amplitude "residue" at the null point due to the error signals, normalized with respect to the pattern maximum, is then

$$E\left[\frac{e_a(x_n,\, y_n)}{a(x_0,\, y_0)}\right] = \frac{\left(\sum_{j=1}^{m}\int_0^q p_j(r)r^2\, dr\right)^{1/2}}{mQ} \quad,$$ (37)

where

  m is the number of array elements,

  q is the quantizer resolution,

  Q is the mean element amplitude, and

  p_j is the probability density of the amplitude of the jth error signal.

Since $p_j(r) = 1/q$ for all j,

$$E\left[\frac{e_a(x_n,\, y_n)}{a(x_0,\, y_0)}\right] = \left(\frac{1}{\sqrt{3m}}\right)\cdot\left(\frac{q}{Q}\right) \quad.$$ (38)

Note that Q is very nearly equal to the peak element amplitude for null positions well displaced from the pattern maximum, and therefore the number of bits "b" of quantization displayed by the quantizer is approximately $\log_2(Q/q)$. In terms of decibels below pattern maximum, the expected value can be expressed as

$$20\log_{10}E\left[\frac{e_a(x_n,\, y_n)}{a(x_0,\, y_0)}\right] \approx -4.8\ dB - 6.0b\ dB - 10\log_{10}m\ dB \quad.$$ (39)

For example, a 1024-element array incorporating 6-bit amplitude quantization would exhibit a filling-in of the null up to a level of about 71 dB below the main beam.

5.3. Phase Quantization

For small phase quantization errors, the error signal introduced at each element is one whose amplitude is given by the product of the phase error and the excitation amplitude, and whose phase is in quadrature with the excitation. Based on the amplitude quantization discussion above, we conclude that the phase-quantization error signal is uniformly distributed in phase, and that it combines with the amplitude-quantization error signal in a root-sum-square manner. Using the same reasoning to find the expected value of the rms amplitude at the null point due to phase-quantization as was used for amplitude quantization, we find

$$E\left[\frac{e_\phi(x_n,\, y_n)}{a(x_0,\, y_0)}\right] = \frac{\left[\sum_{j=1}^{m}\int_0^q P_j(\phi)\phi^2 Q^2\, d\phi\right]^{1/2}}{mQ} = \frac{q}{\sqrt{3m}} \quad,$$ (40)

where q is now the phase quantizer resolution. The phase quantizer must accommodate a range of 2π, which means that the number of bits b is now $\log_2(2\pi/q)$. The expected value now

30

becomes

$$20 \log_{10} E\left[\frac{e_\phi(x_n, y_n)}{a(x_0, y_0)}\right] \approx 11.2 \text{ dB} - 6.0b \text{ dB} - 10 \log_{10} m \text{ dB} \quad . \tag{41}$$

For the same 1024-element array incorporating an 8-bit phase quantizer, phase quantization would degrade null depth to about −67 dB.

5.4. Photodetector Noise

Random photodetector fluctuations ("noise") affect the null depth in a manner similar to the amplitude quantization noise. If the raw photodetector data display an rms noise level of e_n volts, then in the present antenna controller equipment the filtered noise level would be $1.5e_n$, and the processed amplitude output e'_n would be equal to $1.5\sqrt{3}e_n$. The expected value of the rms amplitude of the "residue" at the null position due to noise, normalized with respect to the pattern maximum $a(x_0, y_0)$, is

$$E\left[\frac{a(x_n, y_n)}{a(x_0, y_0)}\right] = \frac{\left[\sum_{j=1}^{m}(e'_n)^2\right]^{1/2}}{mQ} = \left(\frac{1}{\sqrt{m}}\right) \cdot \left(\frac{e'_n}{Q}\right) \quad , \tag{42}$$

where m is the number of photocell elements and Q is the mean photocell amplitude. Expressed in dB, we have

$$20 \log_{10} E\left[\frac{a(x_n, y_n)}{a(x_0, y_0)}\right] = -6.0b_n \text{ dB} - 10 \log_{10} m \text{ dB} \quad , \tag{43}$$

where b_n is the number of bits that e'_n is below Q; thus, $b_n = \log_2(Q/e_n)$. For example, if m is 1024, e_n is 0.012 V, and Q is 2.4 V, then $b_n = 6.3$ and the residue is 68 dB down from peak.

5.5. Fourier Transform Error

Even an ideal lens introduces a nonlinearity in the frequency axis when it is employed to image the Fourier transform of an optical signal. The error is given by Shulman[1] as $(1 - a^2)^{1/2} - 1$, where a is the ratio of displacement from optical axis to lens focal length. For the present antenna controller equipment, a is always less than 0.02 and is less than 0.01 for any appreciable transform density. Thus the error introduced is less than 2×10^{-4} in any case, and less than 5×10^{-5} for practical purposes. This error is insignificant compared to the other errors in the system.

6. COMPONENTS

6.1. Improved E-O Interface

The improved E-O interface, like the existing interface, measures the relative phase and amplitude of an applied optical signal beam at a number of sample points in a plane simultaneously. It outputs electrical signals which are proportional to the phase and amplitudes measured.

---

[1] Arnold R. Shulman, *Optical Data Processing*, New York, John Wiley and Sons (1970), p 185.

The existing interface makes use of an optical reference beam which is mixed with the signal beam. The resultant optical intensity is measured at each sample point and stored. One of the optical beams is then phase shifted a known amount, and the resultant intensity is again measured at each sample point and stored. Four additional phase shifts and intensity measurements are made sequentially, although two are sufficient under certain constraints. From the six sets of intensity measurements, the relative phase and amplitude of the signal beam at each sample point is determined.

As in the existing interface, the improved interface incorporates a means for mixing a reference beam with the signal beam; it makes use of two sets of intensity measurements made with two phases of the reference beam. However, here the sets of intensity measurements are made simultaneously rather than sequentially. Thus, there is no sequential phase shifting, and hence no optical component whose optical length must change with time. As a result, the improved interface not only operates faster but is less complex. The simultaneous taking of both sets of intensity measurements also alleviates problems caused by the drifting of phase in the optical beams. The interface is compact and rugged because of the mechanical configuration of the optical assembly; the mathematical operations that must be executed by the electronic signal processor are quite simple, and in fact may be replaced by a look-up operation.

The improved device comprises an optical assembly, an electronic signal processor, and interconnecting cables. The optical assembly intercepts the signal beam (the beam of interest, which is to be measured) and a reference beam, which also must be provided. As in the existing device, the reference beam must be coherent with the signal beam, a condition which is generally produced by deriving the two beams from the same optical source. Two photodetector arrays incorporated in the optical assembly respond to the intensity of the signal and reference beams as combined in the optical assembly. Electrical signals proportional to these intensities are fed to the electronic signal processor by means of the interconnecting cables. The electronic signal processor operates upon the electrical signals in the prescribed manner so as to form electrical output signals that represent the relative phases and amplitudes of the points measured. The processing operations are done digitally; first, the analog signals from the photodetector arrays are converted into digital signals, and then digital circuitry is used to perform the operations.

Figure 22 is an exploded view of the optical assembly, and shows the optical paths of the signal beam and reference beam. Figure 23 is an assembled view of the optical assembly, and shows where the signal beam and reference beam are applied. Figure 24 is a block diagram of the entire device. As shown in figure 22, the signal beam is incident upon the cube beamsplitter. A fraction of the energy of this beam passes through to the polarizer and photodetector array no. 1, while a like fraction is reflected within the beamsplitter to a second polarizer and photodetector array no. 2.

The reference beam is directed through the quarter-wave plate to the beamsplitter by the prism. A fraction of the energy of the reference beam passes through the beamsplitter to the polarizer and photodetector array no. 1, and a like fraction is reflected within the beamsplitter to the polarizer and photodetector array no. 2. Thus both photodetector arrays are illuminated by both the signal beam and the reference beam.

The signal beam and reference beam are assumed to be vertically polarized where they are incident upon the optical assembly, although any other plane polarization angle could be accom-
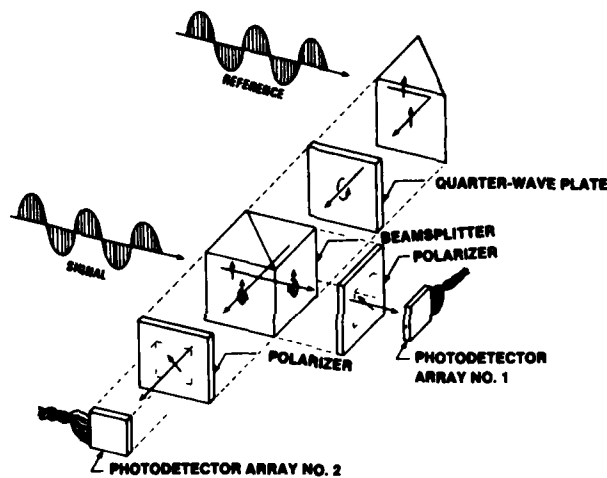
32

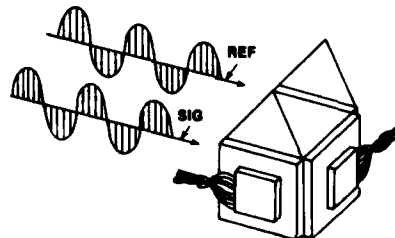Figure 22.   Exploded view of improved E-O interface.

Figure 23.   Improved E-O interface assembly.
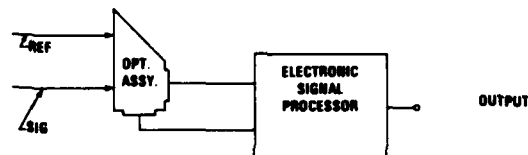
Figure 24.   Block diagram of improved E-O interface.

modated by proper orientation of the quarter-wave plate and the polarizers. The reference beam is assumed to have a cross section large enough to illuminate the photodetector arrays over the area of interest. The reference beam is also assumed to be a plane wave, although perturbations in the measured phase caused by a nonplanar wave could be calibrated out of the system.

As is also shown in figure 22, the reference beam is vertically polarized upon entering and exiting the prism, as is indicated by the vertical arrows on the faces of the prism. The quarter-wave plate is oriented so as to convert the plane-polarized reference beam into a circularly polarized beam, as is indicated by the circular arrow on the face of the quarter-wave plate. The two polarizers resolve the circularly polarized beam into two plane-polarized beams which are π/

33

2 radians out of phase. These polarizers are similarly oriented so that they pass light energy polarized at an angle of $\pi/4$ radians to the vertical, as indicated by the slanted arrows on their faces.

The relative phase shift occurs because the sense of the reference-beam polarization is reversed for the path through the beamsplitter that includes a reflection, but not for the other path, as is indicated by the oppositely directed circular arrows on the exit faces of the beam-splitter. Thus, relative to the beams incident upon the polarizers, the polarizers have planes of polarization which are crossed, which results in beams exiting the polarizers which are plane polarized and relatively phase shifted by $\pi/2$ radians.

The signal beam does not pass through a quarter-wave plate, and therefore it remains plane polarized. The signal beam incident upon each polarizer has vertical polarization and therefore the beam exiting the polarizer in each case is attenuated but not relatively phase shifted.

Both photodetector arrays have incident upon their photosensitive surfaces a combination of signal beam and reference beam, with the reference-beam phase at one photodetector array shifted $\pi/2$ radians with respect to the reference-beam phase at the other photodetector array. Thus two sets of intensity measurements with different reference-beam phases can be obtained simultaneously by the two photodetector arrays. It should be noted that one photodetector array sees a signal image that is reversed right to left with respect to that seen by the second detector array because of the reflection within the beamsplitter in one optical path. A given sample point in the signal beam will therefore appear at different positions in the two photodetector arrays. This shift must be taken into account when the intensity measurements are paired for each sample point. The electrical outputs from the photodetector arrays provide a measure of the optical intensities at each sample point in the signal beam. The electronic signal processor amplifies and digitizes these outputs, and executes the mathematical operations upon them necessary to determine relative phase and amplitude at each sample point.

Let R_1 and R_2 be the instantaneous amplitudes of the combined signal and reference beams at a given sample point at the two photodetector arrays. (All amplitude and intensity values are normalized so that the reference beam by itself would display unity peak amplitude at the photodetector arrays.) If k is the peak signal amplitude at the sample point, and if ϕ is the signal phase relative to the reference beam at one photodetector array and $\phi - \pi/2$ is the signal phase relative to the reference beam at the other photodetector array, then

$$R_1^2 = [\cos \omega t + k \cos(\omega t + \phi)]^2 + [\sin \omega t + k \sin(\omega t + \phi)]^2 \tag{44}$$

and

$$R_2^2 = [\cos(\omega t + \pi/2) + k \cos(\omega t + \phi)]^2 + [\sin(\omega t + \pi/2) + k \sin(\omega t + \phi)]^2 . \tag{45}$$

where ω is the optical frequency in radians per unit time. The corresponding intensities can be found by squaring the amplitudes and integrating over the optical period T:

$$A_1 = 1 + k^2 + 2k \cos \phi , \tag{46}$$

and

$$A_2 = 1 + k^2 + 2k \sin \phi . \tag{47}$$

Now A_1 and A_2 are the quantities directly measured by the photodetector arrays, while k and ϕ

34

are the quantities sought. For convenience the results will be found in terms of θ instead of ϕ, where $\theta = \phi + \pi/4$.

Let us define the sum S and the difference D by

$$S = A_1 + A_2 \quad ,$$

and

$$D = A_1 - A_2 \quad .$$

It then follows that

$$k^2 = (\tfrac{1}{4})S \pm \sqrt{S - (\tfrac{1}{4})D^2 - 1} \quad , \tag{48}$$

and

$$\cos \theta = D/(\sqrt{8}k) \quad . \tag{49}$$

By constraining the allowable input signal intensity so that $0 \le k \le \sqrt{\tfrac{1}{2}}$, the uncertainty of sign in equation (48) is removed, and we have

$$k = \sqrt{(\tfrac{1}{4})S - \sqrt{S - (\tfrac{1}{4})D^2 - 1}} \quad , \tag{50}$$

and

$$S = 2(k^2 + 1) + \sqrt{8}k \sin \theta \quad . \tag{51}$$

Imposing the constraint results in a limit on k given by $k \le (\tfrac{1}{2})S$, which forces the sign of the radical in equation (48) to be negative. It is apparent that in any phase-measuring device employing continuous-wave signal and reference beams, there is an uncertainty in the number of whole cycles of phase that the signal exhibits. Thus the phase can only be expressed as a number of radians modulo 2π. The number thus has a total range of 2π. For convenience, θ will be expressed here as an angle which always lies in the range $-\pi$ to π. Equation (49) can then be expressed as

$$\theta = \arccos[D/(\sqrt{8}k)] \quad , \quad \text{for} \quad S \ge 2(k^2 + 1)$$
$$= -\arccos[D/(\sqrt{8}k)] \quad , \quad \text{for} \quad S < 2(k^2 + 1) \quad . \tag{52}$$

The relationship between the value of S and the sign of the angle θ can be seen by examining equation (51) with positive and negative angles. All the relationships required for determining k and θ under the constraint $0 \le k \le \tfrac{1}{2}$ have been given above. Specifically, the electronic signal processor inputs a measure of A_1 and A_2, forms the sum and difference S and D, computes k by the mathematical operations given by equation (50), compares the value of S with the computed $2(k^2 + 1)$, then performs the appropriate computations for finding θ as given in equation (52). The computed values for k and θ are output for each sample point in the form of digital and/or analog signals as desired.

6.2. Solid-Medium Optical Processor

Coherent optical processors for any application are generally implemented in the form of elements, such as lenses, mirrors, and plates, mounted at appropriate separations on a rigid base. To some extent the elements are cantilevered; in any case the alignments and separations are strongly affected by vibration. Relative changes in path length between signal beam and reference beam must be held to a fraction of a wavelength of the laser source—that is, to about one ten-

thousandth of a millimeter—for the interval in which a set of data frames is taken. Vibration is therefore a problem.

A second problem arises from the existence of airborne dust which even pervades enclosed processors. Processor outputs often exhibit the Fourier transform of one or more large dust particles that have settled on lens or mirror elements.

A third problem arises from multiple reflections from air-glass interfaces throughout the processor, which result in unwanted interference patterns.

Alleviation of these problems may be provided by configuring the processor as one mass of transparent medium, and constraining all optical paths to lie within the medium to the extent possible. Air gaps would only appear where mechanical translation is required, although ultimately these mechanical motions would be eliminated and reprogrammable electro-optic devices (such as the Itek PROM*) would be substituted. Thus, after manufacture, there would be little opportunity for dust to enter the system. There would be few air-glass (or "air-medium") interfaces, and the ridigity of the structure would stabilize optical path lengths.

Figure 25 shows a proposed solid-medium processor. It could readily be fabricated from lenses, prisms, and the like, cemented together. The Fourier-transforming elements would be curved reflective surfaces. The reference and signal beams would progress through the assembly side by side (actually changing sides at each focal plane), then would be combined at the E-O interface.
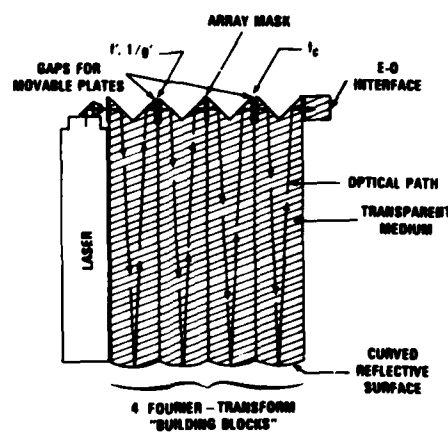

Figure 25.   Solid-medium processor.

---

* Pockels Readout Optical Modulator.

7. CONCLUSIONS

From the analysis and experimental results we may conclude that it is possible to dynamically control the far-field pattern of an array antenna, even to the extent of maintaining a null at an arbitrary position (or multiple nulls at nearly arbitrary positions), by controlling the antenna elements according to the computational algorithms given. The algorithms are attractive in that they incorporate means for independently steering antenna beams and nulls, as well as means for changing beam size and shape.

Secondly, these algorithms can be implemented successfully in a coherent optical processor. While the demonstration equipment was neither small nor fast, design approaches to a compact, rugged, high-speed processor have been outlined.

Thirdly, in order to achieve significantly deep nulls, the antenna under control must incorporate elements which permit fine amplitude and phase control. In existing antennas of small or moderate size this capability is almost never found, primarily because of the expense and complexity involved and the inefficiency arising from any attenuators required. In those instances where the control versatility afforded outweighs these drawbacks, the algorithms and the coherent optical processor implementation should be considered. With the advent of moderate-power, high-frequency, solid-state sources, arrays of radiating elements might be constructed wherein amplitude control takes the form of gain control rather than attenuation, thereby alleviating the power inefficiency problem.

37

APPENDIX A:
EXPERIMENTAL COHERENT OPTICAL PROCESSOR

An experimental coherent optical processor, configured as an antenna controller, was assembled. Figure A-1 shows the significant elements of the processor. The photographic plates are labeled with the functions they represent, as was done in figures 2 and 7 in the body of the report. The Fourier transform elements are 60-cm focal length lenses. In two out of the three primary positions, L1 and L2, telecentric lenses specifically designed for the task are employed. For the third position, L3, which came about through an evolutionary process, no such lens was available.
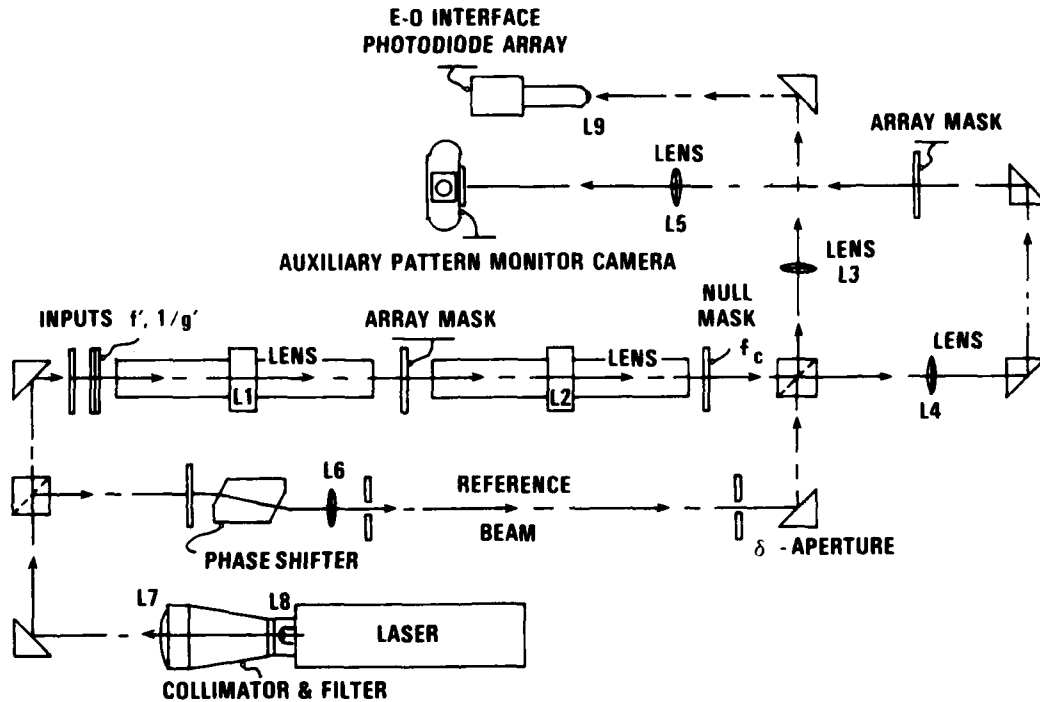

Figure A-1.   Experimental coherent optical processor.

DISTRIBUTION

ADMINISTRATOR
DEFENSE DOCUMENTATION CENTER
ATTN DDC-TCA (12 COPIES)
CAMERON STATION, BUILDING 5
ALEXANDRIA, VA 22314

COMMANDER
US ARMY RSCH & STD GP (EUR)
ATTN LTC JAMES M. KENNEDY, JR.
      CHIEF, PHYSICS & MATH BRANCH
FPO NEW YORK 09510

COMMANDER
US ARMY MATERIEL DEVELOPMENT &
 READINESS COMMAND
ATTN DRXAM-TL, HQ TECH LIBRARY
5001 EISENHOWER AVENUE
ALEXANDRIA, VA 22333

COMMANDER
US ARMY ARMAMENT MATERIEL
 READINESS COMMAND
ATTN DRSAR-LEP-L, TECHNICAL LIBRARY
ROCK ISLAND, IL 61299

COMMANDER
US ARMY MISSILE & MUNITIONS
 CENTER & SCHOOL
ATTN ATSK-CTD-F
REDSTONE ARSENAL, AL 35809

DIRECTOR
US ARMY MATERIEL SYSTEMS
 ANALYSIS ACTIVITY
ATTN DRXSY-MP
ABERDEEN PROVING GROUND, MD 21005

DIRECTOR
US ARMY BALLISTIC RESEARCH LABORATORY
ATTN DRDAR-TSB-S (STINFO)
ABERDEEN PROVING GROUND, MD 21005

TELEDYNE BROWN ENGINEERING
CUMMINGS RESEARCH PARK
ATTN DR. MELVIN L. PRICE, MS-44
HUNTSVILLE, AL 35807

ENGINEERING SOCIETIES LIBRARY
345 EAST 47TH STREET
ATTN ACQUISITIONS DEPARTMENT
NEW YORK, NY 10017

US ARMY ELECTRONICS TECHNOLOGY
 & DEVICES LABORATORY
ATTN DELET-DD
FORT MONMOUTH, NJ 07703

COMMANDER
US ARMY ENGINEER TOPOGRAPHIC LABORATORIES
BLDG 2592
ATTN USAETL-R1, DR. R. D. LEIGHTY
ATTN USAETL-R1, J. BENTON
FORT BELVOIR, VA 22060

COMMANDER
US ARMY BALLISTIC MISSILE DEFENSE
ADVANCED TECHNOLOGY CENTER
ATTN BMDATC-R, BERNARD W. VATZ
HUNTSVILLE, AL 35803

COMMANDER
US ARMY COMMUNICATIONS RESEARCH
 & DEVELOPMENT COMMAND
ATTN DRDCO-COM-RM, I. KULLBACK
FORT MONMOUTH, NJ 07708

DIRECTOR
NAVAL RESEARCH LABORATORY
ATTN 5300 RADAR DIVISION
ATTN 5500 OPTICAL SCIENCE DIVISION
WASHINGTON, DC 20375

COMMANDER
NAVAL SURFACE WEAPONS CENTER·
ATTN DF-36, RADAR SYSTEMS ENGR BR
ATTN DG-30, APPLIED SCIENCE
      & MATERIALS DIVISION
DAHLGREN, VA 22448

COMMANDER
NAVAL SURFACE WEAPONS CENTER
ATTN WA-30, RADAR & FUZING DIVISION
ATTN WR-42, ELECTRO-OPTICS BRANCH
WHITE OAK, MD 20910

COMMANDER
NAVAL WEAPONS CENTER
ATTN 394, ELECTRO-OPTICS DIVISION
CHINA LAKE, CA 93555

DIRECTOR
AF AVIONICS LABORATORY
ATTN KJA(TEO), ELECTRO-OPTICS TECHNOLOGY BR
ATTN KJE(TER), ELECTRONIC RESEARCH BR
WRIGHT-PATTERSON AFB, OH 45433

COMMANDER
HQ ROME AIR DEVELOPMENT CENTER (AFSC)
ATTN LE, DEPUTY FOR ELECTRONIC TECHNOLOGY
GRIFFISS AFB, NY 13441

41

PRECEDING PAGE NOT FILMED
BLANK

DISTRIBUTION (Cont'd)

US ARMY ELECTRONICS RESEARCH
 & DEVELOPMENT COMMAND
 ATTN TECHNICAL DIRECTOR, DRDEL-CT
 ATTN DRDEL-AP-CCM, DR. J. L. SCALES

HARRY DIAMOND LABORATORIES
 ATTN 00100, COMMANDER/TECH DIR/TSO
 ATTN CHIEF, DIV 10000
 ATTN CHIEF, DIV 20000
 ATTN CHIEF, DIV 30000
 ATTN CHIEF, DIV 40000
 ATTN RECORD COPY, 81200
 ATTN HDL LIBRARY, (3 COPIES) 81100
 ATTN HDL LIBRARY, (WOODBRIDGE) 81100
 ATTN TECHNICAL REPORTS BRANCH, 81300
 ATTN CHAIRMAN, EDITORIAL COMMITTEE
 ATTN CHIEF, BR 11140
 ATTN GIESKE, H., 11140
 ATTN CUNEO, J., 11140
 ATTN HEINARD, W. G., 11150
 ATTN LEE, J., 13200
 ATTN CHIEF, BR 15200
 ATTN CHIEF, BR 15300
 ATTN BIEHL, B., 15300
 ATTN CHIEF, BR 15400
 ATTN GEIGER, T., 15400
 ATTN EMMERMAN, P., 15400
 ATTN SWORD, M., 15400
 ATTN SHREVE, J., 15300 (10 COPIES)